

A Toomre-like stability criterion for the clumpy and turbulent interstellar medium

Alessandro B. Romeo,^{1*} Andreas Burkert² and Oscar Agertz³

¹*Onsala Space Observatory, Chalmers University of Technology, SE-43992 Onsala, Sweden*

²*University Observatory, University of Munich, Scheinerstr. 1, D-81679 Munich, Germany*

³*Institute for Theoretical Physics, University of Zürich, CH-8057 Zürich, Switzerland*

Accepted 2010 May 6. Received 2010 April 22; in original form 2010 January 26

ABSTRACT

We explore the gravitational instability of clumpy and turbulent gas discs, taking into account the Larson-type scaling laws observed in giant molecular clouds (GMCs) and H I, as well as more general scaling relations. This degree of freedom is of special interest in view of the coming high- z ISM surveys, and is thus potentially important for understanding the dynamical effects of turbulence at all epochs of galaxy evolution. Our analysis shows that turbulence has a deep impact on the gravitational instability of the disc. It excites a rich variety of stability regimes, several of which have no classical counterpart. Among other diagnostics, we provide *two useful tools* for observers and simulators: (1) the stability map of turbulence, which illustrates our stability scenario and relates it to the phenomenology of interstellar turbulence: GMC/H I observations, simulations and models; (2) a Toomre-like stability criterion, $Q \geq \bar{Q}$, which applies to a large class of clumpy/turbulent discs. We make specific predictions about GMC and cold-H I turbulence, and point out the implications of our analysis for high- z galaxy surveys.

Key words: instabilities – turbulence – ISM: general – ISM: kinematics and dynamics – ISM: structure – galaxies: ISM.

1 INTRODUCTION

Toomre’s (1964) stability criterion, $Q \geq 1$, is one of the pillars of disc galaxy dynamics (see, e.g., Binney & Tremaine 2008). It is used in a wide variety of contexts; in star formation for example, where the gravitational instability of the interstellar gas plays a critical role (e.g., Quirk 1972; Kennicutt 1989; Martin & Kennicutt 2001; Schaye 2004, 2008; Burkert 2009; Elmegreen 2009).

So why introduce a new stability criterion? Because behind Toomre’s criterion there is one fundamental assumption: the medium is approximately in equilibrium, with well-defined surface density Σ and velocity dispersion σ . But this is far from being true in the clumpy and turbulent interstellar gas, where such quantities depend strongly on ℓ , the size of the region over which they are measured. In fact, a fundamental aspect of interstellar turbulence is the existence of density- and velocity-size scaling laws: $\Sigma \propto \ell^a$ and $\sigma \propto \ell^b$ (see, e.g., Elmegreen & Scalo 2004; McKee & Ostriker 2007). In giant molecular clouds (GMCs), the scaling exponents are $a \approx 0$ and $b \approx \frac{1}{2}$ (e.g., Larson 1981; Solomon et al. 1987; Bolatto et al. 2008; Heyer et al. 2009; Hughes et al. 2010).

In the H I component, density and velocity fluctuations seem to have a Kolmogorov spectrum *up to galactic scales*: $a \sim \frac{1}{3}$ for $\ell \lesssim 10$ kpc, and $b \sim \frac{1}{3}$ for $\ell \lesssim 1$ kpc (e.g., Lazarian & Pogosyan 2000; Elmegreen et al. 2001; Begum et al. 2006; Kim et al. 2007; Dutta et al. 2008; Roy et al. 2008; Dutta et al. 2009a, b). Note, however, that the uncertainties are large, especially in the H I case. Further evidence for ISM turbulence is provided by the ‘Big Power Law in the Sky’, i.e. the fact that electron density fluctuations show a Kolmogorov spectrum over a wide range of scales: from 10^3 km up to 10 pc (Armstrong et al. 1995; see Chepurnov & Lazarian 2010 for the most recent determination of the upper scale).

Clumpy and turbulent gas is also observed in high-redshift star-forming galaxies, where it dominates the morphology and dynamics of the disc (e.g., Wadadekar et al. 2006; Elmegreen et al. 2007; Genzel et al. 2008; Shapiro et al. 2008; Förster Schreiber et al. 2009). Coming surveys will tell us how Σ and σ scale with ℓ at high z , and thus how turbulence develops in disc galaxies. This is one of the hot topics in modern astrophysics (e.g., Krumholz & Burkert 2010), and several state-of-the-art simulations have already been designed for such a purpose (e.g., Wada et al. 2002; Kim & Ostriker 2007; Levine et al. 2008; Agertz et al. 2009a, b; Bournaud & Elmegreen 2009; Dekel et al. 2009;

* E-mail: romeo@chalmers.se

Tasker & Tan 2009). In order to interpret such data correctly, one must understand in detail how turbulence affects the (in)stability of the disc.

These facts all together motivate a thorough investigation of the problem.

Elmegreen (1996) assumed Larson-type scaling relations, $\Sigma \propto \ell^a$ and $\sigma \propto \ell^b$, and investigated the case $a = -1$ and $b = \frac{1}{2}$. He found that the disc is always stable at large scales and unstable at small scales. To the best of our knowledge, this was the only theoretical work devoted to the gravitational instability of clumpy/turbulent discs before ours. In contrast, several investigations focused on the effects of turbulence on Jeans instability (e.g., Bonazzola et al. 1987; Just et al. 1994; Vázquez-Semadeni & Gazol 1995).

The goal of our paper is to explore the gravitational instability of clumpy/turbulent discs, spanning the whole range of values for a and b . Among other diagnostics, we provide two useful tools for observers and simulators:

(i) *The stability map of turbulence.* Using a and b as coordinates, we illustrate the natural variety of stability regimes possessed by such discs, and populate this diagram with observations, simulations and models of interstellar turbulence (Fig. 1).

(ii) *A Toomre-like stability criterion.* We show that in our map there is a densely populated domain where the stability criterion is of the form $Q \geq \bar{Q}$, and determine the stability threshold \bar{Q} as a function of a , b and of the scale at which Q is measured [Eq. (17) and Fig. 2]. If our criterion is fulfilled, then the disc is stable at all scales (the case investigated by Elmegreen 1996 lies in another stability regime).

The rest of the paper is organized as follows. In Sect. 2, we determine a dispersion relation that takes fully into account the scaling laws of interstellar turbulence as well as the thickness of the gas layer. We then surf through the various stability regimes. Our Toomre-like stability criterion is given in Sect. 2.7, together with other important diagnostics: the most unstable scale and its growth rate. In Sect. 3, we discuss the stability map of turbulence. We then make specific predictions about strongly and weakly supersonic turbulence. In Sect. 4, we explore the densely populated Toomre-like domain and illustrate the stability diagnostics in a number of cases, taking into account the saturation of density and velocity at large scales. In Sect. 5, we draw the conclusions.

2 STABLE OR UNSTABLE ?

2.1 The turbulent dispersion relation

Consider a gas disc of scale height h , and perturb it with axisymmetric waves of frequency ω and wavenumber k . The response of the disc is described by the dispersion relation

$$\omega^2 = \kappa^2 - \frac{2\pi G \Sigma k}{1 + kh} + \sigma^2 k^2, \quad (1)$$

where κ is the epicyclic frequency, Σ is the surface density at equilibrium, and σ is the sound speed (Romeo 1990, 1992, 1994; see also Vandervoort 1970). So the three terms on the right side of Eq. (1) represent the contributions of rotation, self-gravity and pressure. For $kh \ll 1$, Eq. (1) reduces to the usual dispersion relation for an infinitesimally thin gas

disc (see, e.g., Binney & Tremaine 2008). For $kh \gg 1$, one recovers the case of Jeans instability with rotation, since $\Sigma/h \approx 2\rho$. In other words, scales comparable to h mark the transition from 2D to 3D stability. Note that we can encapsulate the effect of thickness in a single quantity and rewrite Eq. (1) as

$$\omega^2 = \kappa^2 - 2\pi G \Sigma_{\text{eff}} k + \sigma^2 k^2, \quad (2)$$

where $\Sigma_{\text{eff}} = \Sigma/(1 + kh)$ is the effective surface density. Σ_{eff} and σ are two important quantities, which we discuss in detail below.

The effective surface density. What is the relation between Σ_{eff} and ρ ? Since $\Sigma_{\text{eff}} = \Sigma/(1 + kh)$ and $\Sigma \sim \rho h$, we find that $\Sigma_{\text{eff}} \sim \rho h$ if $kh \lesssim 1$, and $\Sigma_{\text{eff}} \sim \rho/k$ otherwise. This means that the observational counterpart of Σ_{eff} is the mass column density measured over a region of size $\ell = 1/k$. In the cold ISM, which is highly supersonic and hence strongly compressible, the amplitude of density fluctuations is typically much larger than the mean density. Density fluctuations have a power-law energy spectrum, $E_\rho(k) \propto k^{-r}$, which means $\rho \propto k^{-(r-1)/2}$ (see, e.g., Elmegreen & Scalo 2004). A power-law spectrum is then imprinted on Σ_{eff} :

$$\Sigma_{\text{eff}} = \Sigma_0 \left(\frac{k}{k_0} \right)^{-a}. \quad (3)$$

Using the relation between Σ_{eff} and ρ that we have found above, we can relate a to r : $a = \frac{1}{2}(r - 1)$ for $kh \lesssim 1$, while $a = \frac{1}{2}(r + 1)$ for $kh \gtrsim 1$. In the warm ISM, which is transonic or subsonic and hence weakly compressible, the density contrast is typically small so Σ_{eff} is dominated by the mean density, as in the limiting case of a non-turbulent disc: $\Sigma_{\text{eff}} = \text{constant}$ for small k , while $\Sigma_{\text{eff}} \propto k^{-1}$ for large k . Hereafter we will omit the subscript ‘eff’, unless otherwise stated.

The sound speed. The observational counterpart of σ is the 1D velocity dispersion measured over a region of size $\ell = 1/k$: $\sigma^2 = \sigma_{\text{ther}}^2 + \sigma_{\text{tur}}^2(k)$, where σ_{ther} and σ_{tur} are the thermal and turbulent 1D velocity dispersions. Velocity fluctuations have a power-law energy spectrum, $E_v(k) \propto k^{-s}$, which means $\sigma_{\text{tur}} \propto k^{-(s-1)/2}$ (see, e.g., Elmegreen & Scalo 2004). Both thermal and turbulent motions tend to support the gas against gravitational instability. However, as pointed out by the referee, turbulent support results in relations that are true only in a statistical sense, with individual clouds collapsing even when the statistical criterion for stability is well satisfied. In the cold ISM, σ has a power-law dependence on k since it is dominated by $\sigma_{\text{tur}}(k)$:

$$\sigma = \sigma_0 \left(\frac{k}{k_0} \right)^{-b}, \quad (4)$$

where $b = \frac{1}{2}(s - 1)$ and s is the velocity spectral index. In the warm ISM, $\sigma(k)$ deviates significantly from a power law since σ_{ther} is no longer negligible.

Hereafter we will only consider the *cold* ISM (H_2 and cold H I), since in such a case we can explicitly take into account the power-law scaling of interstellar turbulence via Eqs (3) and (4). We will regard the quantity $\ell_0 = 1/k_0$ introduced in those equations as the fiducial scale at which the mass column density and the 1D velocity dispersion are observed. This is also the scale at which Q and other stability

quantities are measured. Substituting Eqs (3) and (4) into Eq. (2), we obtain the final dispersion relation:

$$\omega^2 = \kappa^2 - 2\pi G \Sigma_0 k_0^a k^{1-a} + \sigma_0^2 k_0^{2b} k^{2(1-b)}. \quad (5)$$

Our phenomenological approach differs significantly from the traditional way to include turbulent effects in the dispersion relation, which is to identify σ with the typical 1D velocity dispersion observed at galactic scales. Bonazzola et al. (1987), Just et al. (1994), Vázquez-Semadeni & Gazol (1995) and Elmegreen (1996) adopted an approach similar to ours for investigating the gravitational instability of clumpy/turbulent media.

Eq. (5) is the starting-point of our stability analysis. As in the usual case, stability at all scales requires that $\omega^2 \geq 0$ for all k .¹ Whether this requirement can be satisfied or not depends on the self-gravity and pressure terms, which now scale as k^A and k^B :

$$A = 1 - a, \quad (6)$$

$$B = 2(1 - b). \quad (7)$$

In the following, we explore all the various cases.

2.2 Case $a = 1, b \neq 1$

Here the self-gravity term is independent of k ($A = 0$), like the rotation term:

$$\omega^2 = \underbrace{\kappa^2 - 2\pi G \Sigma_0 k_0}_C + \sigma_0^2 k_0^{2b} k^{2(1-b)}. \quad (8)$$

For $b < 1$, ω^2 increases with k and tends to C as $k \rightarrow 0$. Hence the sign of C determines whether the disc is stable at all scales or not. Stability requires that $C \geq 0$. For $b > 1$, ω^2 decreases with k and tends to C as $k \rightarrow \infty$. So, again, stability requires that $C \geq 0$. The stability criterion is then:

$$\text{STABLE } \forall k \iff k_0 \leq k_T = \frac{\kappa^2}{2\pi G \Sigma_0}. \quad (9)$$

Eq. (9) resembles Toomre's stability criterion for cold discs, $k \leq k_T$, but there is one important difference: Eq. (9) is a condition that must be fulfilled by k_0 to ensure stability for all k , whereas the cold Toomre criterion ensures stability for small k .

2.3 Case $a \neq 1, b = \frac{1}{2}(1 + a)$

Here the pressure term has the same k -dependence as the self-gravity term ($B = A$):

$$\omega^2 = \kappa^2 + \underbrace{(\sigma_0^2 k_0^{1+a} - 2\pi G \Sigma_0 k_0^a)}_C k^{1-a}. \quad (10)$$

¹ The dispersion relation assumes that $kR \gg 1$, where R is the radial coordinate (see, e.g., Binney & Tremaine 2008). This local condition is more restrictive than the natural requirement $k \gtrsim 2\pi/L$, where L is the size of the gas disc. Since the condition above cannot be rigorously included in the stability analysis, the usual procedure is to consider all k and to check a posteriori whether $kR \gg 1$ or not.

If $a < 1$, then ω^2 converges to κ^2 as $k \rightarrow 0$ and the sign of $d\omega^2/dk$ is equal to the sign of C (for $C < 0$, ω^2 diverges as $k \rightarrow \infty$). Hence stability requires that $C \geq 0$. If $a > 1$, then ω^2 converges to κ^2 as $k \rightarrow \infty$ and the sign of $d\omega^2/dk$ is opposite to the sign of C (for $C < 0$, ω^2 diverges as $k \rightarrow 0$). So, again, stability requires that $C \geq 0$. The stability criterion is then:

$$\text{STABLE } \forall k \iff k_0 \geq k_J = \frac{2\pi G \Sigma_0}{\sigma_0^2}. \quad (11)$$

The resemblance between Eq. (11) and the 2D Jeans criterion, $k \geq k_J$, is superficial. In fact, Eq. (11) ensures that the disc is stable at all, rather than small, scales. An analogous fact was noted in the context of our first stability criterion [Eq. (9)].

2.4 Case $a = 1, b = 1$

Although this case seems the intersection of Case 2.2 and Case 2.3, the stability criterion is not $k_J \leq k_0 \leq k_T$. In fact, this case is singular. The self-gravity and pressure terms are independent of k ($A = B = 0$), like the rotation term, so $\omega^2(k)$ is constant:

$$\omega^2 = \underbrace{\kappa^2 - 2\pi G \Sigma_0 k_0 + \sigma_0^2 k_0^2}_C. \quad (12)$$

As C is quadratic in k_0 , the inequality $C \geq 0$ can be easily solved and the resulting stability criterion is:

$$\text{STABLE } \forall k \iff \begin{cases} k_0 \leq k_- \text{ or } k_0 \geq k_+ & \text{if } Q < 1, \\ 0 < k_0 < \infty & \text{else.} \end{cases} \quad (13)$$

Here k_- and k_+ are related to the Toomre wavenumber k_T (and to the Jeans wavenumber $k_J = k_T 4/Q^2$):

$$k_{\pm} = k_T \frac{2}{Q^2} \left(1 \pm \sqrt{1 - Q^2} \right); \quad (14)$$

and Q is the Toomre parameter:

$$Q = \frac{\kappa \sigma_0}{\pi G \Sigma_0}. \quad (15)$$

The $Q < 1$ case of Eq. (13) resembles the corresponding Toomre stability condition, but see the remarks following Eqs (9) and (11). In contrast, the $Q \geq 1$ case is identical to Toomre's criterion.

2.5 Case $a < 1, b > \frac{1}{2}(1 + a)$

Now $A > 0$ and $B < A$. Hence the self-gravity term gets dominant for large k and makes ω^2 negative. For small k , ω^2 is positive since it is dominated by the pressure term ($B < 0$) and/or the rotation term ($B \geq 0$). As the zero(s) of $\omega^2(k)$ can only be determined numerically, case by case, we do not give a stability criterion but note that the disc is *unstable at small scales*, like a cold non-turbulent disc.

2.6 Case $a > 1, b < \frac{1}{2}(1 + a)$

In contrast to the previous case, $A < 0$ and $B > A$. So ω^2 is dominated by the self-gravity term and is negative for small k , while it is dominated by the pressure/rotation term and is positive for large k . Thus the disc is *unstable at large scales*, like a non-rotating non-turbulent sheet.

2.7 Case $a < 1$, $b < \frac{1}{2}(1+a)$

When $0 < A < B$, the response of the disc is driven by pressure at small scales and by rotation at large scales, while self-gravity acts more strongly at intermediate scales. Therefore this is a Toomre-like case: $\omega^2(k)$ has a minimum, which determines whether the disc is stable or not. More precisely, the minimum of $\omega^2(k)$ provides three useful pieces of information: the stability threshold, the most unstable scale and its growth rate. Such quantities are introduced below, while illustrative cases are discussed in Sect. 4.

The *stability threshold* \bar{Q} is the value of Q above which the disc is stable at all scales:

$$\text{STABLE } \forall k \iff Q \geq \bar{Q}. \quad (16)$$

\bar{Q} can be determined by imposing that the minimum of $\omega^2(k)$ vanishes. Even though the calculations are very lengthy, the formula is simple, especially if expressed in terms of the ‘right’ parameters:

$$\bar{Q} = 2 \left[A^A B^{-B} (B-A)^{B-A} \left(\frac{\ell_0}{\ell_T} \right)^{2A-B} \right]^{1/(2A)}, \quad (17)$$

where $\ell_T = 1/k_T$ is the Toomre scale. Eq. (16), with \bar{Q} specified by Eq. (17), is our stability criterion. It reduces to Toomre’s criterion $Q \geq 1$ in the limiting case of a non-turbulent disc: $A = 1$, $B = 2$ ($a = b = 0$).

The *most unstable scale*, $\ell_{\min} = 1/k_{\min}$, is given by the formula:

$$\frac{\ell_{\min}}{\ell_T} = \bar{\mathcal{L}} (Q/\bar{Q})^{2/(B-A)}, \quad (18)$$

where Q/\bar{Q} measures the stability level of the disc (like Q in Toomre’s case), and $\bar{\mathcal{L}}$ is the value of ℓ_{\min}/ℓ_T at the stability threshold ($Q/\bar{Q} = 1$):

$$\bar{\mathcal{L}} = \left[\frac{B-A}{B} \left(\frac{\ell_0}{\ell_T} \right)^{A-1} \right]^{1/A}. \quad (19)$$

Eq. (18) reduces to $\ell_{\min}/\ell_T = \frac{1}{2} Q^2$ in Toomre’s case.

The *growth rate of the most unstable scale*, $\gamma_{\min} = (-\omega_{\min}^2)^{1/2}$, is given by the formula:

$$\frac{\omega_{\min}^2}{\kappa^2} = 1 - (Q/\bar{Q})^{-2A/(B-A)}, \quad (20)$$

which vanishes at the stability threshold. Eq. (20) reduces to $\omega_{\min}^2/\kappa^2 = 1 - Q^{-2}$ in Toomre’s case.

2.8 Case $a > 1$, $b > \frac{1}{2}(1+a)$

Even $B < A < 0$ is a Toomre-like case. In fact, although the scales at which pressure and rotation dominate are reversed, self-gravity still controls intermediate scales and $\omega^2(k)$ has a minimum, which determines whether the disc is stable or not. This means that, even now, the stability criterion is:

$$\text{STABLE } \forall k \iff Q \geq \bar{Q}. \quad (21)$$

The stability threshold \bar{Q} , the most unstable scale and its growth rate, ℓ_{\min} and γ_{\min} , are given by the same formulae as in Eqs (17)–(20).

3 THE STABILITY MAP OF TURBULENCE

The results of Sect. 2 are summarized in Fig. 1. The (a, b) plane is divided into four regions, where stability à la Toomre alternates with instability at small or large scales. The two shaded lines that separate those regions, and the point at which those lines intersect, represent transitions between different stability phases. Thus the corresponding stability criteria are hybrid (see Sects 2.2–2.4). The points $(a, b) = (0, 0)$ and $(a, b) = (-1, \frac{1}{2})$ represent the limiting case of a non-turbulent disc and the case investigated by Elmegreen (1996). To the best of our knowledge, this was the only theoretical work devoted to the gravitational instability of clumpy/turbulent discs before ours. Fig. 1 also illustrates the most interesting stability regimes populated by models, simulations and observations of astrophysical turbulence. Such points are discussed throughout the rest of this section. Specific predictions about strongly and weakly super-sonic turbulence are then made in Sect. 3.1.

The mass-size scaling relation, $M \propto \Sigma \ell^2 \propto \ell^{a+2}$, tells us the natural bounds of a . In fact, $D = a + 2$ is the fractal dimension of the mass distribution, which ranges from 0 to 3, so we have $-2 \leq a \leq 1$. Note that the upper bound corresponds to the case in which the destabilizing effect of self-gravity is scale-independent, i.e. to the vertical shaded line introduced above.

Does even the other shaded line have a twofold meaning? Yes, and an important one! If the stabilizing effect of pressure has the same scale-dependence as the effect of self-gravity, $b = \frac{1}{2}(1+a)$, then $\sigma^2 \propto \ell \Sigma \propto M/\ell$, which is the virial scaling relation. GMCs are then expected to clump along that line, i.e. to populate the transition regime between stability à la Toomre and instability at small scales. For example, the well-known scaling laws $\Sigma = \text{constant}$ and $\sigma \propto \ell^{1/2}$ (Larson 1981; Solomon et al. 1987) correspond to the point $(a, b) = (0, \frac{1}{2})$. Both Galactic and extragalactic GMCs show non-negligible dispersion around that point, especially along the virial line, as can be inferred from Bolatto et al. (2008) and Heyer et al. (2009). The case of perturbed galactic environments seems different. Rosolowsky & Blitz (2005) investigated the physical properties of GMCs in M64 (NGC 4826), an interacting molecule-rich galaxy, and found $\Sigma \propto M^{0.7 \pm 0.2}$ and $\sigma \propto \ell^{1.0 \pm 0.3}$, which means $(a, b) = (5_{-3}^{+13}, 1.0 \pm 0.3)$. If such scaling relations apply to individual GMCs, as was originally suggested, then each cloud is far from being in simple virial equilibrium. Besides, since (a, b) is below the virial line and on the right of the $a = 1$ line, the H_2 disc is unstable at large scales (in the sense specified in Sect. 2.6) and the fractal dimension is formally higher than three. Alternatively, one may argue that those scaling relations arise from the superposition of more GMCs, each one characterized by the standard scaling laws, but with proportionality factors varying significantly over the disc (Rosolowsky, private communication).

Now what about HI? A turbulence model that is becoming more and more popular is the one introduced by Fleck (1996), which predicts $\rho^{1/3} \sigma \propto \ell^{1/3}$. To understand the meaning of this scaling relation, compare it with Kolmogorov’s law $\sigma \propto \ell^{1/3}$. Fleck’s relation tells us that in a turbulent medium with both velocity and density fluctuations the quantity $\rho^{1/3} \sigma$ plays a role similar to σ in incompressible turbulence. Fleck (1996) assumed that $\Sigma \sim \rho \ell$,

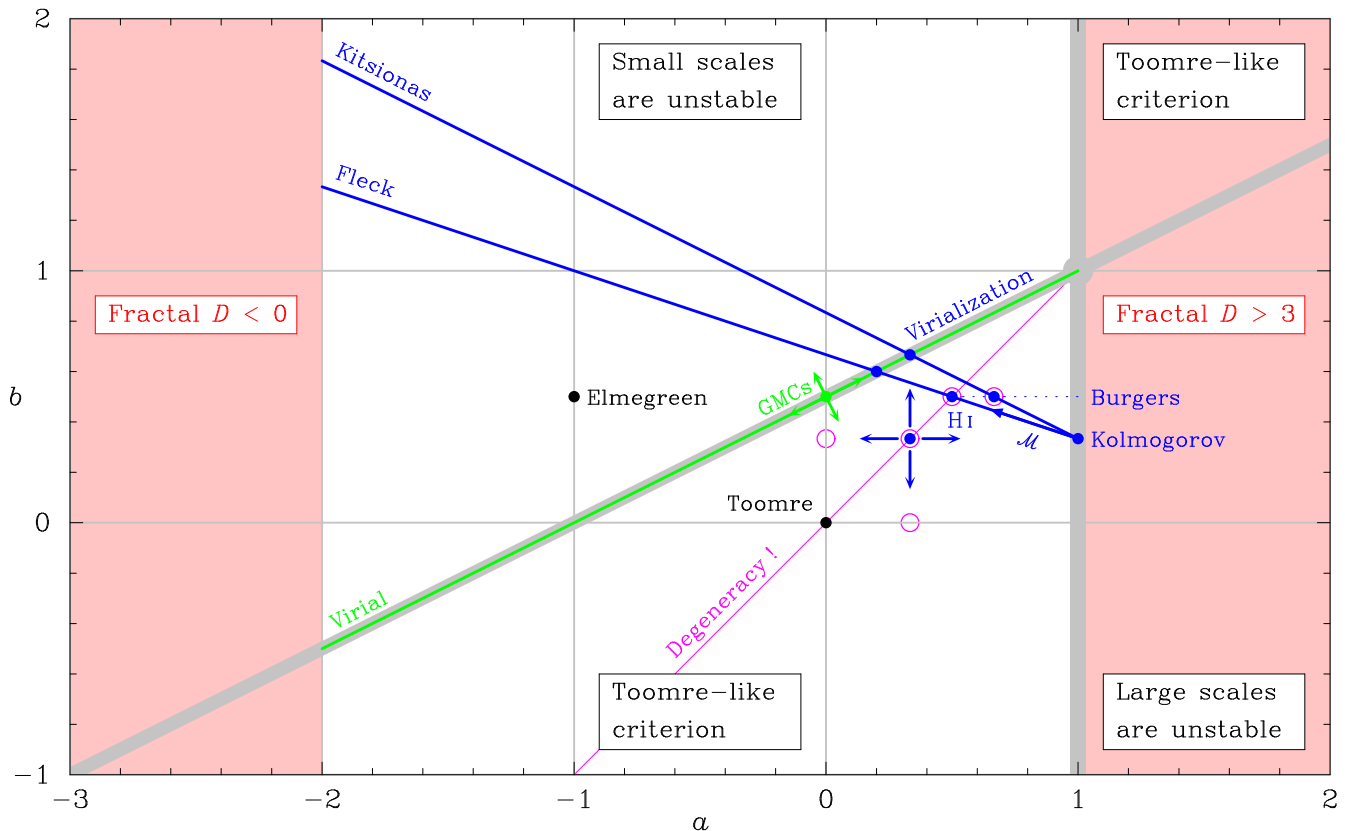


Figure 1. The stability map of turbulence. The coordinates a and b are the exponents of the density- and velocity-size scaling relations [see Eqs (3) and (4)]. The shaded lines, their intersection point and the regions between them represent the variety of stability regimes possessed by clumpy/turbulent discs. The points $(a, b) = (0, 0)$ and $(a, b) = (-1, \frac{1}{2})$ correspond to the limiting case of a non-turbulent disc and to the case investigated by Elmegreen (1996). The non-shaded part of the plane shows the natural range of a . The thick lines are phenomenological models of GMC and H I turbulence, the semiclosed-head arrows represent observations, while the closed-head arrow represents simulations with increasing Mach number. The solid circles correspond to points of special interest in astrophysical turbulence. Also shown are the cases illustrated in Figs 2 and 3 (hollow circles), and the degeneracy condition discussed in Sect. 4 (thin line). Note that the stability criterion is $Q \geq 1$ along such a line.

which means $\ell \lesssim h$ (see Sect. 2.1). So his prediction corresponds to the line $b = \frac{1}{3}(2 - a)$, which crosses several stability regimes. The limiting case of Kolmogorov turbulence, $(a, b) = (1, \frac{1}{3})$, lies in the transition regime between stability à la Toomre and instability at large scales. Both high-resolution simulations of supersonic turbulence and H I observations populate the Toomre-like domain. Such simulations cluster along the Fleck line, near $(a, b) = (\frac{1}{2}, \frac{1}{2})$, the case of Burgers turbulence (Kowal & Lazarian 2007; Kritsuk et al. 2007; Schmidt et al. 2008; Price & Federrath 2010; see also Fleck 1996 and references therein). In weakly supersonic regimes, simulations cluster closer to the Kolmogorov limit $(a, b) = (1, \frac{1}{3})$, as we will show in Sect. 3.1. Observed H I intensity fluctuations, which are primarily due to *cold*² H I (Lazarian & Pogosyan 2000), show large scatter around $(a, b) = (\frac{1}{3}, \frac{1}{3})$, i.e. suggest a Kolmogorov scaling for both velocity and density fluctuations (e.g., Lazarian & Pogosyan 2000; Elmegreen et al. 2001; Begum et al. 2006; Dutta et al. 2008, 2009a, b). Such a scaling is also consistent with other H I observations (e.g., Kim et al. 2007; Roy et al. 2008). The

simulations by Agertz et al. (2009a), designed to explore the development of H I turbulence in disc galaxies, suggest power-law indices consistent with the observed ones, except before the fragmentation of the disc (Agertz, Romeo et al., in preparation).

Note that there is a very interesting and unexpected case where Fleck’s model fits the observations well: the transition from H I to GMC turbulence. Clumps that climb up the Fleck line become progressively more self-gravitating and will virialize at $(a, b) = (\frac{1}{5}, \frac{3}{5})$. This is close to $(a, b) = (0, \frac{1}{2})$, the reference point for GMC observations. The predicted energy spectra are $E_\Sigma(k) \propto d\Sigma^2/dk \propto k^{-7/5}$ and $E_\sigma(k) \propto d\sigma^2/dk \propto k^{-11/5}$ (the Kolmogorov spectrum scales as $k^{-5/3}$).

Low-resolution simulations of supersonic turbulence suggest an alternative scaling relation: $\rho^{1/2}\sigma \propto \ell^{1/3}$ (Kitsionas et al. 2009). In comparison with the Fleck case, this scaling gives more weight to density fluctuations and translates into a steeper line: $b = \frac{1}{2}(\frac{5}{3} - a)$, where it is again assumed that $\Sigma \sim \rho\ell$. The cases of Kolmogorov and Burgers turbulence correspond to $(a, b) = (1, \frac{1}{3})$ and $(a, b) = (\frac{2}{3}, \frac{1}{2})$, while the virialization point is $(a, b) = (\frac{1}{3}, \frac{2}{3})$. The Kitsionas line crosses the same stability regimes as the Fleck line, but lies farther away from H I and GMC observations.

² Hereafter we will omit ‘cold’ when referring to H I, since our analysis also focuses on the cold ISM (see Sect. 2.1).

3.1 Strongly vs. weakly supersonic turbulence

Although our analysis focuses on strongly supersonic turbulence (see Sect. 2.1), here we extend it to weakly supersonic regimes (the case of a transonic or subsonic medium was considered in Sect. 2.1).

How does the Mach number affect the density- and velocity-size scaling relations? And how does it affect the stability of the disc? To answer these questions, one should not compute a and b directly from the density and velocity spectral indices. One should first evaluate the typical density contrast of the medium (see Sect. 2.1). The density probability distribution is approximately lognormal, and its mean μ and standard deviation SD depend on the rms Mach number \mathcal{M} (Padoan et al. 1997): $\mu = \frac{1}{2}\text{SD}^2 \approx \frac{1}{2} \ln(1 + \frac{1}{4}\mathcal{M}^2)$. For such a distribution, the mass-weighted median density is $\rho_{\text{med}} = \bar{\rho} e^{\mu} \approx \bar{\rho} (1 + \frac{1}{4}\mathcal{M}^2)^{1/2}$, where $\bar{\rho}$ is the mean density (see sect. 2.1.4 of McKee & Ostriker 2007). This provides a robust estimate of the typical density (mean plus fluctuations) in the medium. The corresponding density contrast is $\delta_{\text{med}} = (\rho_{\text{med}} - \bar{\rho})/\bar{\rho}$.

In weakly supersonic turbulence ($\mathcal{M} \approx 2$), we have $\delta_{\text{med}} \approx 0.4$ so the mass column density at scale ℓ is dominated by the mean density: $\Sigma_{\text{eff}} \approx \bar{\rho} \ell$ (hence $a \approx 1$) for $\ell \lesssim h$, while $\Sigma_{\text{eff}} \approx \bar{\rho} h$ (hence $a \approx 0$) for $\ell \gtrsim h$. In contrast, the 1D velocity dispersion at scale ℓ is dominated by the turbulent term: $\sigma \approx \sigma_{\text{tur}}(\ell) \propto \ell^b$. For $\ell \lesssim h$, we can relate b to a using Fleck's model, $b = \frac{1}{3}(2 - a)$, and get $(a, b) \approx (1, \frac{1}{3})$. Thus weakly supersonic 3D turbulence drives the disc to the boundary of the Toomre-like domain, near the Kolmogorov point.

In strongly supersonic turbulence ($\mathcal{M} \gtrsim 5$), we have $\delta_{\text{med}} \gtrsim 2$ so both the mass column density and the 1D velocity dispersion are dominated by turbulent fluctuations. We can then compute a and b from the density and velocity spectral indices (see Sect. 2.1). Simulations show that in an isothermal medium with negligible self-gravity, with or without magnetic fields, the density spectrum flattens (Beresnyak et al. 2005; Kim & Ryu 2005; Kowal et al. 2007) and the velocity spectrum steepens (e.g., Kowal & Lazarian 2007; Kritsuk et al. 2007; Price & Federrath 2010) as the Mach number increases. At Mach 7, we find $(a, b) \sim (0.8, 0.4)$ from Kowal et al. (2007) and $(a, b) \sim (0.3, 0.6)$ from Kowal & Lazarian (2007), using Fleck's model in both cases.³ In spite of the large uncertainties, it is clear that these points are on the left of $(1, \frac{1}{3})$ and, on average, closer to $(\frac{1}{2}, \frac{1}{2})$. Thus strongly supersonic 3D turbulence drives the disc well inside the Toomre-like domain, near the Burgers point.

³ In the first case, $d \ln E_\rho / d \ln k$ (i.e. $-r$) is given in table 2 of Kowal et al. (2007); a is computed from r as in Sect. 2.1 ($\ell \lesssim h$): $a = \frac{1}{2}(r + 1)$; and b is computed from a using Fleck's model: $b = \frac{1}{3}(2 - a)$. This yields $(a, b) = (0.75 \pm 0.05, 0.42 \pm 0.02)$ for the sub-Alfvénic simulation and $(a, b) = (0.80 \pm 0.10, 0.40 \pm 0.03)$ for the super-Alfvénic simulation. In the second case (of the main text), $d \ln E_v / d \ln k$ (i.e. $-s$) is given in fig. 1 of Kowal & Lazarian (2007); b is computed from s as in Sect. 2.1: $b = \frac{1}{2}(s - 1)$; and a is computed from b using Fleck's model: $a = 2 - 3b$. This yields $(a, b) = (0.29 \pm 0.08, 0.57 \pm 0.03)$. This simulation is sub-Alfvénic, like the first one above.

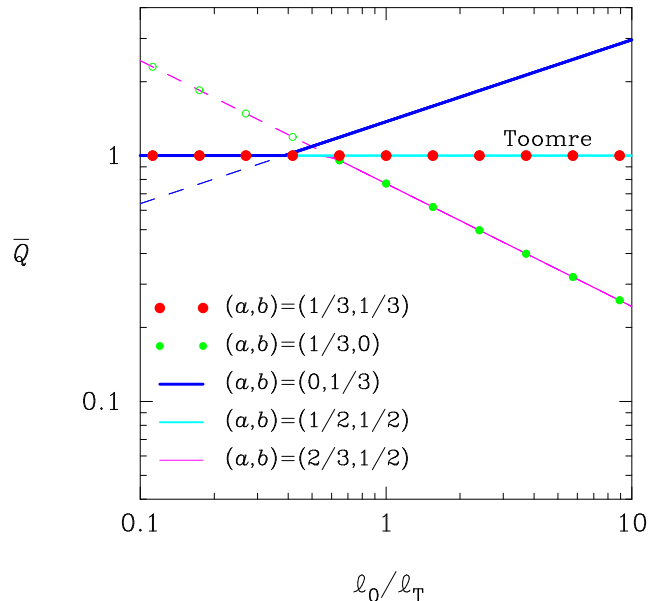


Figure 2. The stability threshold of clumpy/turbulent discs, $\bar{Q} = \bar{Q}(a, b, \ell_0)$, where a and b are the exponents of the density- and velocity-size scaling relations, and ℓ_0 is the typical scale at which density and velocity saturate. In addition, ℓ_T is the Toomre scale. The dashed lines and the hollow circles show the power-law behaviour predicted by Eq. (17) when density and velocity do not saturate; ℓ_0 is then the fiducial scale at which those quantities are observed. The limiting case of a non-turbulent disc is $\bar{Q} = 1$.

4 ILLUSTRATIVE CASES

Let us now illustrate the stability characteristics of clumpy/turbulent discs in a number of cases, those marked with hollow circles in the Toomre-like domain of our map (see Fig. 1). The points $(\frac{1}{3}, \frac{1}{3})$, $(\frac{1}{2}, \frac{1}{2})$ and $(\frac{2}{3}, \frac{1}{2})$ are typical values of (a, b) inferred from HI observations, high- and low-resolution simulations of supersonic turbulence. The points $(\frac{1}{3}, 0)$ and $(0, \frac{1}{3})$ are the contributions of density and velocity fluctuations to the observed $(a, b) = (\frac{1}{3}, \frac{1}{3})$. For each case, we proceed in two ways. First, we assume that the density- and velocity-size scaling relations are perfect power laws, as given by Eqs (3) and (4), so that $\ell_0 = 1/k_0$ is the fiducial scale at which density and velocity are observed. We then evaluate the stability characteristics analytically using Eqs (17)–(20). Second, we consider more realistic scaling relations, which take into account the saturation of density and velocity at large scales:

$$\Sigma_{\text{eff}} = \Sigma_0 \mathcal{D}_\ell, \quad \mathcal{D}_\ell = \begin{cases} (\ell/\ell_0)^a & \text{if } \ell \leq \ell_0, \\ 1 & \text{else;} \end{cases} \quad (22)$$

$$\sigma = \sigma_0 \mathcal{V}_\ell, \quad \mathcal{V}_\ell = \begin{cases} (\ell/\ell_0)^b & \text{if } \ell \leq \ell_0, \\ 1 & \text{else;} \end{cases} \quad (23)$$

where ℓ_0 is now the typical saturation scale. We then evaluate the stability characteristics numerically using the dispersion relation, Eq. (2), which we rewrite as:

$$\frac{\omega^2}{\kappa^2} = 1 - \frac{\mathcal{D}_\ell}{(\ell/\ell_T)} + \frac{Q^2}{4} \frac{\mathcal{V}_\ell^2}{(\ell/\ell_T)^2}, \quad (24)$$

where $Q = \kappa \sigma_0 / \pi G \Sigma_0$ is the Toomre parameter and $\ell_T = 2\pi G \Sigma_0 / \kappa^2$ is the Toomre scale.

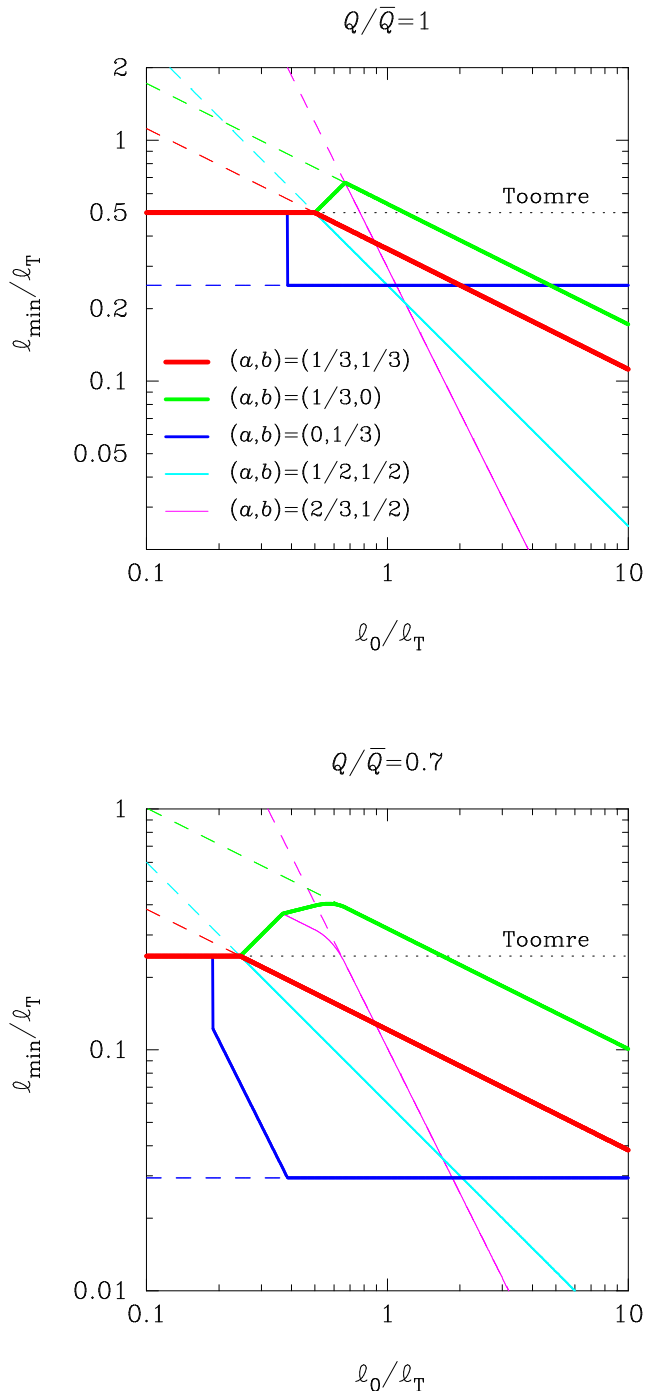


Figure 3. The most unstable scale of clumpy/turbulent discs, $\ell_{\min} = \ell_{\min}(a, b, \ell_0, Q/\bar{Q})$, where a and b are the exponents of the density- and velocity-size scaling relations, ℓ_0 is the typical scale at which density and velocity saturate, and Q/\bar{Q} is the stability level. In addition, ℓ_T is the Toomre scale. The dashed lines show the power-law behaviour predicted by Eqs (18) and (19) when density and velocity do not saturate; ℓ_0 is then the fiducial scale at which those quantities are observed. Also shown is the limiting case of a non-turbulent disc (dotted line).

Fig. 2 shows the stability threshold \bar{Q} , i.e. the value of Q above which the disc is stable at all scales. The first curious result is that such a diagnostic is highly degenerate. For example, look at the cases $(a, b) = (\frac{1}{3}, \frac{1}{3})$ and $(a, b) = (\frac{1}{2}, \frac{1}{2})$, which represent H I observations and high-resolution simulations of supersonic turbulence. They have $\bar{Q} \equiv 1$! Why do such cases degenerate into Toomre’s case? Why doesn’t turbulence show up? Eq. (17) gives us the answer: because the effects of density and velocity fluctuations cancel out when $2A - B = 0$, i.e. along the line $b = a$ (see the map). The cases $(a, b) = (\frac{1}{3}, 0)$ and $(a, b) = (0, \frac{1}{3})$ allow us to disentangle such effects. Density fluctuations that saturate at a typical scale ℓ_0 tend to stabilize the disc by decreasing the stability threshold: $\bar{Q} < 1$ if $\ell_0 \gtrsim \frac{1}{2}\ell_T$, and $\bar{Q} = 1$ otherwise. To understand this result, remember that such fluctuations reduce the self-gravity term in the dispersion relation by a factor \mathcal{D}_ℓ [see Eqs (22) and (24)], and that self-gravity is destabilizing. Velocity fluctuations have an antagonistic effect. They reduce pressure by a factor \mathcal{V}_ℓ^2 [see Eqs (23) and (24)], and tend to destabilize the disc by increasing the stability threshold: $\bar{Q} > 1$ if $\ell_0 \gtrsim \frac{1}{2}\ell_T$, and $\bar{Q} = 1$ otherwise. When density/velocity fluctuations do not saturate, their effect becomes destabilizing/stabilizing if the fiducial scale is small.

Fig. 3 shows the most unstable scale, ℓ_{\min} , for two values of Q/\bar{Q} . Remember that this quantity measures the stability level of the disc, like Q in Toomre’s case. So $Q/\bar{Q} = 1$ (top panel) means that the disc is marginally unstable, while $Q/\bar{Q} = 0.7$ (bottom panel) means that the disc is moderately unstable. In contrast to \bar{Q} , ℓ_{\min} is not degenerate. Turbulence now has a significant effect in the case of H I observations, since the contributions of density and velocity fluctuations are no longer antagonistic. For $\ell_0 \sim \ell_T$, ℓ_{\min} is about 30 to 50 per cent smaller than in Toomre’s case, depending on the value of Q/\bar{Q} . The impact of turbulence is stronger in the case of high-resolution simulations: the most unstable scale is typically half an order of magnitude below the expected value. Turbulent effects become less important at low resolution.

The growth rate of the most unstable scale, γ_{\min} , is independent of ℓ_0 and vanishes for $Q/\bar{Q} = 1$ [see Eq. (20)]. For $Q/\bar{Q} < 1$, the effects of density and velocity fluctuations cancel out when $A/(B - A) = 1$, i.e. $b = a$. This degeneracy condition is the same as that found for \bar{Q} , and has the same consequences.

5 CONCLUSIONS

- Observations and simulations of the interstellar medium are revealing its turbulent nature with higher and higher fidelity. Such information must then be taken into account when analysing the stability of galactic discs. Our contribution is a natural extension to Toomre’s work, which will prove useful for both low- and high-redshift analyses.

- Turbulence has a deep impact on the gravitational instability of the disc. It excites a rich variety of stability regimes, several of which have no classical counterpart. We illustrate this result in the form of a map, which relates our stability scenario to the phenomenology of interstellar turbulence: GMC/H I observations, simulations and models.
- GMC turbulence drives the disc to a regime of tran-

sition between instability at small scales and stability à la Toomre. Toomre's criterion works instead typically well when applied to discs of cold H I, since the effects of density and velocity fluctuations tend to cancel out. Even so, H I turbulence produces a clear signature in disc morphology. It reduces the characteristic scale of instability by 30–50 per cent or more, depending on the value of Q and on the shape of the energy spectrum. The transition from H I to GMC turbulence occurs when $\Sigma \sim \ell^{1/5}$ and $\sigma \sim \ell^{3/5}$ (for more information see Sect. 3).

• Coming astronomical facilities such as ALMA⁴ will be able to resolve the scaling properties of galactic turbulence up to very high redshifts. Using our map, such data will show up as *evolutionary tracks*, which will reveal the interplay between gravitational instability and turbulence during the galaxy life. In turn, this will be useful for constraining the sources of galactic turbulence and for understanding the evolution of cosmic star formation.

ACKNOWLEDGMENTS

We are very grateful to John Black, Leo Blitz, Rick Hestman, Ben Moore and Erik Rosolowsky for useful discussions. We are also grateful to an anonymous referee for constructive comments and suggestions. The first author thanks Bruce Elmegreen for strong encouragement and valuable feedback on the occasion of the IAU Symposium 254 ‘The Galaxy Disk in Cosmological Context’. He also thanks the warm hospitality of both the Department of Physics at the University of Gothenburg and the Department of Fundamental Physics at Chalmers.

REFERENCES

- Agertz O., Lake G., Teyssier R., Moore B., Mayer L., Romeo A. B., 2009a, MNRAS, 392, 294
 Agertz O., Teyssier R., Moore B., 2009b, MNRAS, 397, L64
 Armstrong J. W., Rickett B. J., Spangler S. R., 1995, ApJ, 443, 209
 Begum A., Chengalur J. N., Bhardwaj S., 2006, MNRAS, 372, L33
 Beresnyak A., Lazarian A., Cho J., 2005, ApJ, 624, L93
 Binney J., Tremaine S., 2008, Galactic Dynamics. Princeton University Press, Princeton
 Bolatto A. D., Leroy A. K., Rosolowsky E., Walter F., Blitz L., 2008, ApJ, 686, 948
 Bonazzola S., Falgarone E., Heyvaerts J., Péroul M., Puget J. L., 1987, A&A, 172, 293
 Bournaud F., Elmegreen B. G., 2009, ApJ, 694, L158
 Burkert A., 2009, in Andersen J., Bland-Hawthorn J., Nordström B., eds, Proc. IAU Symp. 254, The Galaxy Disk in Cosmological Context. Cambridge Univ. Press, Cambridge, p. 437
 Chepurnov A., Lazarian A., 2010, ApJ, 710, 853
 Dekel A., Sari R., Ceverino D., 2009, ApJ, 703, 785
 Dutta P., Begum A., Bharadwaj S., Chengalur J. N., 2008, MNRAS, 384, L34
 Dutta P., Begum A., Bharadwaj S., Chengalur J. N., 2009a, MNRAS, 397, L60
 Dutta P., Begum A., Bharadwaj S., Chengalur J. N., 2009b, MNRAS, 398, 887
 Elmegreen B. G., 1996, in Block D. L., Greenberg J. M., eds, New Extragalactic Perspectives in the New South Africa. Kluwer, Dordrecht, p. 467
 Elmegreen B. G., 2009, in Andersen J., Bland-Hawthorn J., Nordström B., eds, Proc. IAU Symp. 254, The Galaxy Disk in Cosmological Context. Cambridge Univ. Press, Cambridge, p. 289
 Elmegreen B. G., Scalo J., 2004, ARA&A, 42, 211
 Elmegreen B. G., Kim S., Staveley-Smith L., 2001, ApJ, 548, 749
 Elmegreen D. M., Elmegreen B. G., Ravindranath S., Coe D. A., 2007, ApJ, 658, 763
 Fleck R. C. Jr., 1996, ApJ, 458, 739
 Förster Schreiber N. M., Genzel R., Bouché N. et al., 2009, ApJ, 706, 1364
 Genzel R., Burkert A., Bouché N. et al., 2008, ApJ, 687, 59
 Heyer M., Krawczyk C., Duval J., Jackson J. M., 2009, ApJ, 699, 1092
 Hughes A., Wong T., Ott J. et al., 2010, preprint (arXiv:1004.2094)
 Just A., Jacobi S., Deiss B. M., 1994, A&A, 289, 237
 Kennicutt R. C. Jr., 1989, ApJ, 344, 685
 Kim J., Ryu D., 2005, ApJ, 630, L45
 Kim S., Rosolowsky E., Lee Y. et al., 2007, ApJS, 171, 419
 Kim W.-T., Ostriker E. C., 2007, ApJ, 660, 1232
 Kitsionas S., Federrath C., Klessen R. S. et al., 2009, A&A, 508, 541
 Kowal G., Lazarian A., 2007, ApJ, 666, L69
 Kowal G., Lazarian A., Beresnyak A., 2007, ApJ, 658, 423
 Kritsuk A. G., Norman M. L., Padoan P., Wagner R., 2007, ApJ, 665, 416
 Krumholz M., Burkert A., 2010, preprint (arXiv:1003.4513)
 Larson R. B., 1981, MNRAS, 194, 809
 Lazarian A., Pogosyan D., 2000, ApJ, 537, 720
 Levine R., Gnedin N. Y., Hamilton A. J. S., Kravtsov A. V., 2008, ApJ, 678, 154
 Martin C. L., Kennicutt R. C. Jr., 2001, ApJ, 555, 301
 McKee C. F., Ostriker E. C., 2007, ARA&A, 45, 565
 Padoan P., Jones B. J. T., Nordlund Å. P., 1997, ApJ, 474, 730
 Price D. J., Federrath C., 2010, preprint (arXiv:1004.1446)
 Quirk W. J., 1972, ApJ, 176, L9
 Romeo A. B., 1990, Stability and Secular Heating of Galactic Discs. PhD thesis, SISSA, Trieste, Italy
 Romeo A. B., 1992, MNRAS, 256, 307
 Romeo A. B., 1994, A&A, 286, 799
 Rosolowsky E., Blitz L., 2005, ApJ, 623, 826
 Roy N., Peedikakkandy L., Chengalur J. N., 2008, MNRAS, 387, L18
 Schaye J., 2004, ApJ, 609, 667
 Schaye J., 2008, in Davies J. I., Disney M. J., eds, Proc. IAU Symp. 244, Dark Galaxies and Lost Baryons. Cambridge Univ. Press, Cambridge, p. 247
 Schmidt W., Federrath C., Klessen R., 2008, Phys. Rev. Lett., 101, 194505
 Shapiri K. L., Genzel R., Förster Schreiber N. M. et al., 2008, ApJ, 682, 231
 Solomon P. M., Rivolo A. R., Barrett J., Yahil A., 1987, ApJ, 319, 730
 Tasker E. J., Tan J. C., 2009, ApJ, 700, 358
 Toomre A., 1964, ApJ, 139, 1217
 Vandervoort P. O., 1970, ApJ, 161, 87
 Vázquez-Semadeni E., Gazol A., 1995, A&A, 303, 204
 Wada K., Meurer G., Norman C. A., 2002, ApJ, 577, 197
 Wadadekar Y., Casertano S., de Mello D., 2006, AJ, 132, 1023

This paper has been typeset from a \TeX / \LaTeX file prepared by the author.

⁴ <http://www.eso.org/sci/facilities/alma/>